Influence of Micro-scale Uncertainties on the Reliability of Fibre-Matrix Composites

Sadik L. Omairey[a]*, Peter D. Dunning[a], and Srinivas Sriramula[ab]
[a] School of Engineering, University of Aberdeen, AB24 3UE, United Kingdom
[b] Lloyd's Register Foundation (LRF) Centre for Safety & Reliability Engineering, University of Aberdeen, Aberdeen, AB24 3UE, United Kingdom
* Corresponding author: s.omairey@abdn.ac.uk, https://www.abdn.ac.uk/engineering/people/profiles/s.omairey

Abstract

This study investigates the effect of micro-scale geometric and material property uncertainties on the elastic properties and reliability of fibre reinforced composite materials. Composite materials are often designed using conservative design factors to account for a limited understanding of how multi-scale uncertainties effect reliability. Structural reliability analysis can produce more efficient designs, but requires an understanding of how all sources uncertainty effect probability of failure. Previous studies have not considered micro-scale geometrical uncertainties and their combinations in a multi-scale probabilistic-based reliability framework. Thus, this study will investigate the effect of numerous combinations of micro-scale material property and geometric uncertainties on the homogenised elastic properties. Furthermore, to account for the effect in a reliability-based framework, a novel surrogate modelling technique is developed to represent the uncertainties efficiently. The study concluded that the geometrical fibre stacking uncertainty is as influential as the widely investigated constituent material stiffness uncertainties. Consequently, representing the micro-scale geometric uncertainties within the developed multi-scale probabilistic-based framework improves the estimated stiffness. Thus probability of failure is reduced, compared with considering material property uncertainties only. Moreover, the framework clarified and highlighted the importance of representing fibre geometrical stacking uncertainty for a deeper understanding of their effect on composite stiffness properties.

Keywords: FRP; Uncertainty; RVE Homogenisation; Surrogate model; Reliability

1. Introduction

Composite materials are being used widely in many industries for the improved stiffness-weight ratio compared with alloys. However, the heterogeneous nature and the manufacturing process of composites open the door to many material and geometrical uncertainties to occur within all scales [1]. Thus, composites are often designed with high factors of safety to ensure reliability [2, 3]. To avoid imposing such high factors of safety, it is important to detect and quantify the effect of these uncertainties at their occurrence scale and propagate their effect into higher scales of the composite component. Thus, a clear understanding of the overall composite properties under all possible uncertainties can be obtained. Clarifying this could lead to safer designs and more efficient use of composites.

In Fibre Reinforced Polymer composites (FRP), micro-scale is the smallest scale where the contribution of all constituent materials occurs. It is usually presented as a Representative Volume Element (RVE) as defined by Hill [4]. The micro-scale is an important building block for the composite as it is used to estimate the effective elastic properties used in higher scales [1]. Therefore, much research has been carried out to account for the effect of uncertainties at this scale. For instance, a recent study investigated the uncertainty of constituent materials properties and their probabilistic propagation from micro-scale to upper scales [5]. In addition to material uncertainty, other studies looked into the effect of some geometrical uncertainties in failure related behaviour using larger RVEs (containing many fibres). For example, a numerical study by Brockenbrough et al. [6] looked into the deformation behaviour of edge-stacked square fibres, square diagonal-stacking of square fibres, and triangle-stacking of hexagonal fibres. Based on observed effects, the study concluded that reliable methods need to be developed that account for the distribution of fibres to ensure reproducibility of composite properties. Another study by Nikopour [7] addressed 2D modelling of matrix/voids ratio uncertainty by systematic matrix absence between fibres and its deterministic effect on the elastic properties. A study by Huang [8] focused on the effect of random and systematic fibre placement within an RVE on elastic properties, again in a deterministic approach, where it was concluded that all arrangements have a similar effect. It is important to note that Huang used a large RVE that is computationally prohibitive to use in a probabilistic framework, compared with the small RVE (single fibre) employed by Zhou et al. [5] and Wang et al. [9].

Small RVEs can be used in a probabilistic perspective that require using Monte Carlo simulation (MCS) with reasonable computational time.

From the above, it can be seen that several uncertainties were investigated. However, the joint effect of these uncertainties together in a small RVE that can be used within a multi-scale reliability analysis was not fully examined. Therefore, the first phase of this study starts by covering the effect of individual and joint geometrical and material property uncertainties on the estimation of the composite's effective elastic properties (see Fig. 1). Two categories of geometrical uncertainty are modelled within small 3D RVEs; fibre stacking configurations, and fibre cross-sectional shape. These uncertainties are examined with two material property uncertainties to indicate the significance of each type of uncertainty. The elastic properties are calculated with the commonly used unified periodic RVE homogenisation method [10]. The joint effect of several sources of uncertainty creates many combinations, each having its own effect on the elastic properties. To understand which uncertainty(ies) and combination(s) are influential, the study employs a sensitivity method that can deal with combinations and normalises their effects to highlight the most influential uncertainties and combinations. To achieve this, a factorial design sensitivity method is used [11].

Once the most influential uncertainties are identified, the study investigates the effect of these uncertainties on the probability of failure for different laminate design criteria, namely buckling, vibration, and bending (see Fig. 1). To achieve this efficiently, surrogate models are created that link uncertain parameters to elastic properties. Thus, repeated use of computationally expensive 3D RVEs is avoided during the reliability analysis. Probabilities of failure are then computed using Monte Carlo Simulation (MCS). A Global Sensitivity Analysis (GSA) is also used to evaluate the influence of each uncertainty on the reliability of the composite.

This study is structured to address the effect of micro-scale geometric and material uncertainties on the elastic properties and reliability of fibre reinforced composite materials. In sections 2 and 3 the micro-scale uncertainties and numerical techniques used in the study are explained, respectively. Section 4 presents and discusses results for the effect and sensitivity of uncertainties on stiffness properties, followed by surrogate model creation and finally results on the influence of uncertainties on structural reliability. Section 5 draws conclusions from the observations and results, highlighting the key findings.

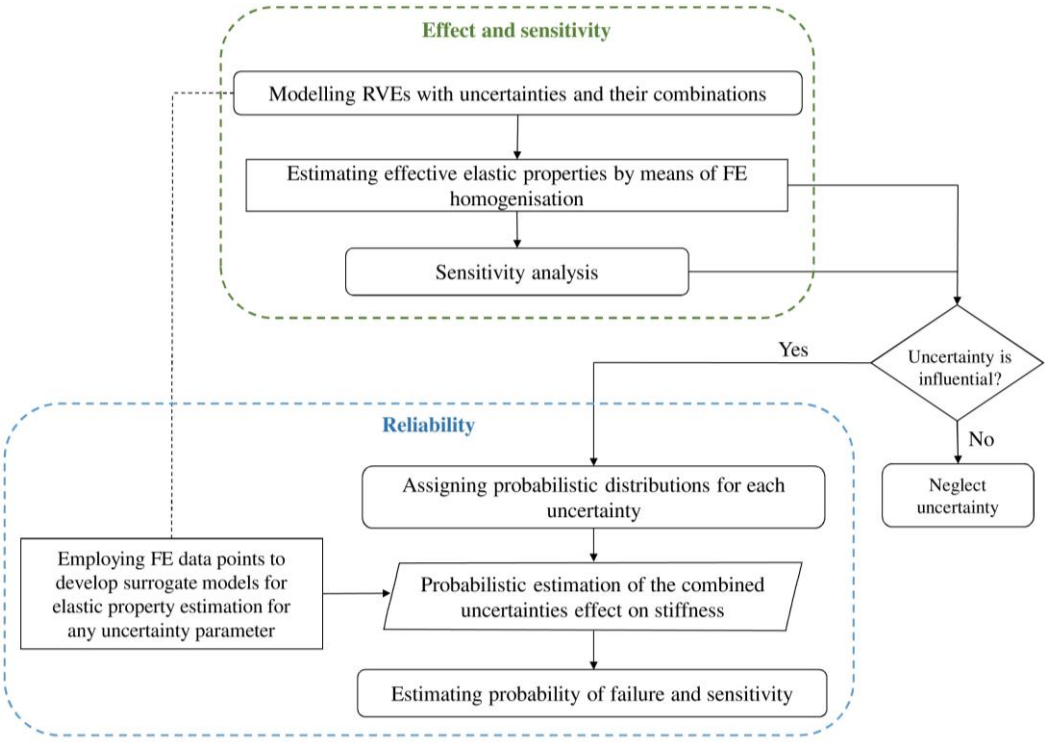

Fig. 1. Probabilistic framework capable of representing geometric and material property uncertainties.

2. Micro-scale uncertainties

Continuous fibre-reinforced composites are generally two-phase heterogeneous materials; fibre phase builds the main strength, whereas matrix phase forms the essential media that holds fibres together. These composites are manufactured using several techniques such as pultrusion, filament winding, and prepreg production processes [12, 13]. All of which introduce a level of uncertainty within constituent phases in terms of material property and geometrical uncertainties [14, 15]. In this study, the continuous fibre-reinforced composites example used is a Boron-Aluminium composite with the properties shown in Table 1. The considered uncertainties are explained in sections 2.1-2.4.

Table 1. Mean material properties and assumed volume ratio of Boron-Aluminium composite [14].

	Elastic modulus E (GPa)	**Poisson's ratio ν**	**Modelled volume ratio**	**Fibre Dia./RVE edge length**
Fibre (Boron)	379.3	0.1	≅0.56	0.3/1.0
Matrix (Aluminium)	68.3	0.3	≅0.44	

In order to highlight the most influential uncertainties and their combinations, a 2^k factorial design approach is used (2, k are a factorial method and the number of factors respectively). This method is generally used with experimental data when many factors effect a response. For composites applications, it was used by Komeili and Milani [1] to evaluate the effect of both material and geometrical uncertainty in woven composite fabric at meso-scale. The 2^k factorial design method requires an upper (positive) and lower (negative) bound to represent each input [11]. Hence, it is assumed that lower bounds (negative effect) of all uncertainties are represented in a deterministic RVE, whereas the positive upper bounds are detailed next in sections 2.1-2.4. For the present study, a total of eight uncertainties are examined, which make sixty possible RVE combinations (as not all uncertainties can occur in combination). All homogenised elastic properties from each model are estimated using RVE homogenisation method (section 3), normalised and presented on normal probability plots, where the most influential uncertainty(ies)/combination(s) are those furthest from the theoretical normal distribution line. In addition, the sensitivity of the selected influential uncertainties on laminate stiffness reliability is assessed using Sobol's [16] global sensitivity indices within a structural reliability framework. A generic Matlab toolbox based on Sobol's approach is used to calculate the sensitivity indices [17].

2.1. Fibre stiffness uncertainty (F uncertainty)

Studies and tests show that fibre strength and stiffness vary around mean values set by manufactures [18]. However, it is difficult to quantify the distribution of such variation due to many factors, such as manufacturing process, type of raw material, quality control measures, testing method, etc. Therefore, literature generally assumes that stiffness is normally distributed around a mean value. In this study, it is assumed that fibre Young's modulus uncertainty (or the positive effect F) is a 5% increase in the deterministic value (the negative effect). As for the effect on reliability, it is assumed that this uncertainty is normally distributed with stiffness mean equal to the deterministic value, and 10% coefficient of variation.

2.2. Matrix stiffness uncertainty (M uncertainty)

More defects can occur in the matrix compared with fibre phase, such as air voids, lumps, insufficient curing. In the current work, matrix uncertainty upper level (positive factor) is again assumed 5% higher than the initial value of the deterministic RVE. For the effect on reliability, it is also assumed that this uncertainty is normally distributed with the deterministic stiffness as the mean, and 10% coefficient of variation.

2.3. Fibres stacking (X and 45 uncertainties)

Fibres are stacked within the matrix phase randomly, which can be seen in various micro-scale Scanning Electron Microscope (SEM) images, as illustrated in Fig. 2 [6, 19-21]. Some studies highlighted the effect of stacking configurations on elastic properties. Again, mostly limited to 2D models using large RVEs that are difficult to use with reliability related studies. Furthermore, many effects on stiffness properties were not examined using sensitivity and reliability analysis. Thus, initially

this study investigates fibres modelled with two stacking position uncertainties. The first stacking uncertainty is shifting the central fibre by 0.06 fraction of the RVE's edge length along 3-direction (*X* uncertainty). Whereas the second is the same amount of shifting but along both 2 and 3-directions (*45* uncertainty), as this creates a +45° off-centre shift. These two uncertainties cannot occur in a single combination, as each represents a distinct case. The negative effect of these stacking uncertainties is the fibre positioned at the centre, as modelled in a deterministic RVE. These two factors represent most stacking possibilities, especially if the axes are rotated. The above stacking configurations (*X*, *45*, and the deterministic model) can be seen in Fig. 3 with the black centre-line representing the original fibre centre, and the yellow representing shifted centre. Conversely, while investigating the effect on reliability, a third off-centre shift in the 2-direction is introduced and explained in section 4.2 and Fig. 11. It is important to highlight that fibre shifting changes the fibre/matrix distribution within the RVE, yet no contact between fibre sections will occur. Additionally, this change is purely geometric with no variation of the overall fibre-volume ratio V_f.

2.4. Fibre shape (S uncertainty)

Fibres are not perfectly circular with a constant cross-sectional area as generally assumed [21]. The illustration in Fig. 2 shows how fibres can change in cross-sectional shape and diameter. This effect was investigated by Ferreira et al. [22] in a two-scale hierarchical optimisation study, where fibre shape was set as a design parameter allowing it to take either circular or elliptical shape. A clear influence of the fibre shape and fibre-volume ratio was observed. For the present study, it is assumed that fibres can take an elliptical shape with the major radius increased by 5% of the standard radius while decreasing the minor radius to maintain a constant fibre cross-sectional area (approximately by 4.7%). Elliptical fibres are rotated around the centre to represent four individual possible geometrical shape uncertainties (*S1*, *S2*, *S3* and *S4*) depending on the angle of their major and minor axes (see Fig. 3). Similar to stacking uncertainty, shape uncertainties do not meet in a single RVE as a combination because each represents a unique case. However, they can be combined with stacking and/or material property uncertainties.

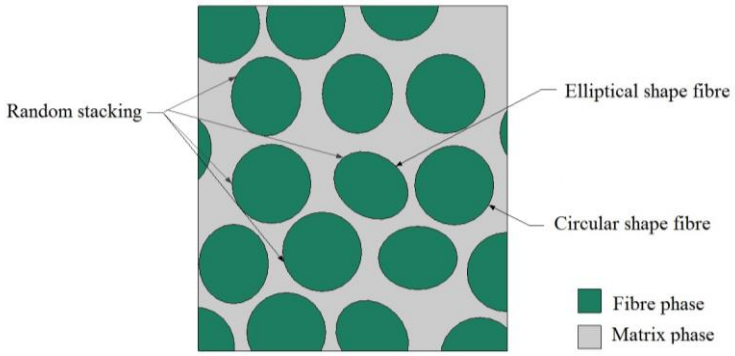

Fig. 2. Representation of fibres' stacking and cross-sectional shape randomness, similar to observations seen in SEM images [6, 20, 21, 23].

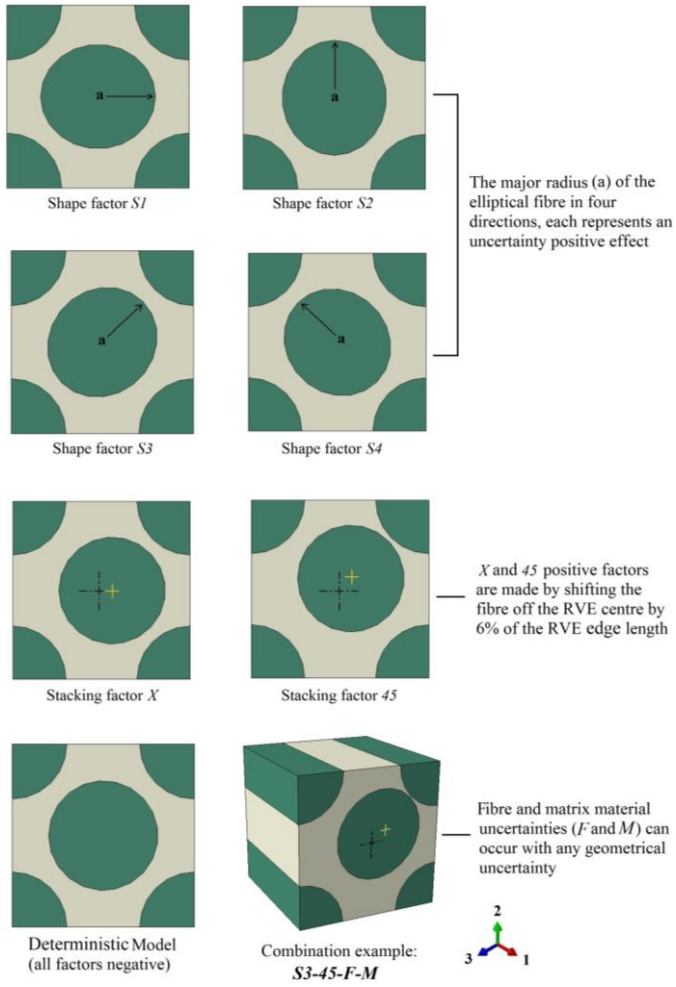

Fig. 3. Scheme of geometric uncertainties and combination sample.

3. RVE homogenisation method

RVE homogenisation method is widely used to predict the effective elastic properties of composite materials for its clear mechanical conception and simplicity [24]. Furthermore, Zhou et al. [25] suggested that this method is becoming the standard approach for composites, as it can analyse general geometries and nonlinear materials [26]. Using an RVE homogenisation method is necessary for this study, as other widely known homogenisation methods such as Chamis (1983) and Mori-Tanaka (1973) are incapable of capturing the effect of geometrical uncertainties/variations.

The concept of RVE homogenisation is numerically imposing uniform strains to compute the effective elastic properties. Generally, these strains are applied in several independent sets of displacements, and each set calculates a specific elastic material property (see Fig. 4). As the RVE is assumed to be part of a periodic material, therefore, it is important to simulate the periodicity of the RVE with the surrounding material before and after being strained in FE software. Earlier homogenisation studies achieved periodicity by imposing boundary conditions that ensure RVE's plane sections remain plane after deformation [6, 27]. However, this is only correct for a transversely isotropic RVE under longitudinal and transverse strains and is not correct for an orthotropic RVE and for shear moduli estimation; since it over-constrains the RVE, leading to overestimating composites' properties. Thus, it is necessary to apply node-to-node periodic conditions at which the deformed boundary surfaces can distort and no longer remain planes [28, 29]. To achieve this, a plugin developed for ABAQUS CAE FE analysis software (ABAQUS Inc. 2013) by the authors' is used to automate the process of computing effective elastic properties of a fully-customised RVE [30].The tool calculates the effective elastic properties by applying the necessary constraint equations and imposing appropriate boundary displacements to satisfy the unified periodicity conditions, based on the concept of periodic RVE

homogenisation [10]. The homogenised elastic properties obtained using this tool came to good agreement with established experimental data for a 0.47 V_f ratio of the selected composite material [28]. In addition, tool outputs are verified against other available commercial FE homogenisation software, as detailed in Omairey et al. [30].

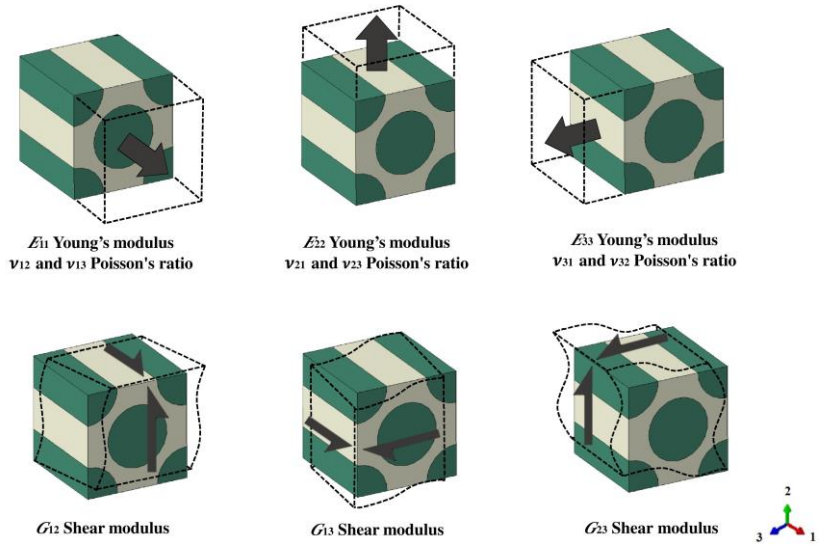

Fig. 4. Schematic representation of displacement boundary conditions required to estimate the effective elastic properties.

The numerical error associated with RVE homogenisation caused by the finite element discretization is investigated so that an appropriate maximum mesh size can be chosen. Four different mesh sizes are used to compute the effective elastic properties of an RVE, where mesh size is stated as a fraction of the RVE edge length. A trend line is then used to estimate the true elastic properties by extrapolating to a mesh size of zero. The estimated true values are then used as a reference point to calculate an estimated error for each mesh size, as shown in Fig. 5 for Young's modulus in the 2-direction (E_{22}) using linear wedge elements. Based on this study, a maximum mesh size of 0.04 is used for RVE discretization, as it gives an acceptable balance between accuracy and computational efficiency.

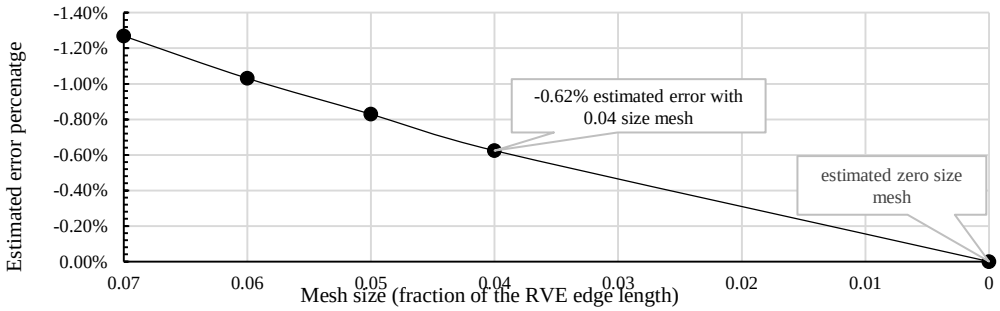

Fig. 5. Four-point mesh convergence line with the estimated error plotted against mesh size for E_{22}.

4. Results and discussions

4.1. Uncertainties effect and sensitivity

Sixty RVEs with various uncertainties are used to compute elastic properties of the composite, while the fibre-volume ratio V_f remains constant. Elastic properties are determined using the RVE homogenisation method described earlier. The effect of individual uncertainties on homogenised properties, as a percentage of the deterministic model, are presented in Table 2. In the following discussions, elastic strain energy (ELSE) is used as an indicator of constituent material contribution to the resistance of applied strains, as it represents work stored inside the material as a result of applied strains and body forces [31].

Table 2. Individual uncertainties effect on the effective elastic properties.

	Stacking uncertainty		Fibre shape uncertainty				Material uncertainty	
Elastic property	***X***	***45***	***S1***	***S2***	***S3***	***S4***	***F***	***M***
E_{11}	0.01%	0.03%	0.00%	0.00%	0.00%	0.00%	4.37%	0.63%
E_{22}	2.12%	3.03%	-0.10%	0.28%	0.03%	0.03%	1.28%	3.63%
E_{33}	0.64%	3.05%	0.27%	-0.10%	0.02%	0.02%	1.28%	3.63%
G_{12}	2.13%	1.73%	-0.64%	0.76%	0.11%	0.12%	1.58%	3.32%
G_{13}	-0.56%	1.71%	0.74%	-0.66%	0.12%	0.10%	1.58%	3.32%
G_{23}	-1.04%	-2.08%	-0.17%	-0.17%	0.23%	0.24%	1.94%	2.96%
v_{12}	-1.38%	-0.50%	0.25%	-0.28%	-0.06%	-0.05%	-0.17%	0.17%
v_{13}	0.90%	-0.53%	-0.28%	0.25%	-0.05%	-0.05%	-0.16%	0.17%
v_{21}	0.70%	2.50%	0.15%	0.00%	-0.05%	-0.05%	-3.12%	3.16%
v_{23}	-1.13%	-4.64%	-0.31%	0.05%	0.10%	0.10%	1.25%	-1.27%
v_{31}	1.56%	2.49%	-0.01%	0.16%	-0.04%	-0.05%	-3.12%	3.16%
v_{32}	-3.05%	-4.61%	0.05%	-0.33%	0.09%	0.10%	1.25%	-1.27%

4.1.1. Effect of geometrical uncertainty

The largest effect on Young's moduli E_{22} and E_{33} is an increase of 3.5% compared with deterministic model values. This occurs by the joint effect of *S3-45* uncertainties. This combination led to an increased stress on the stiffer fibre rather than matrix when resisting the applied strain, making the RVE stiffer in the effected directions. This can be understood by comparing the fibre/matrix strain energy ratio between *S3-45* and the deterministic model, as illustrated in Fig. 6. It is clear that the fibre has more strain energy in *S3-45* model compared with the deterministic model, meaning that the fibre is playing a larger part in resisting the applied unit strains for E_{22} and E_{33}. On the other hand, there is no effect on E_{11} because none of the investigated geometric uncertainties change the fibre-matrix volume ratio in the 1-direction.

As for shear moduli, both increases and decreases are observed. The maximum increase is 3% on G_{12} caused by *S2-X* uncertainties. This arrangement creates a semi-continuous fibre distribution aligned with 2-direction (refer to Fig. 3) that raises the stress on the stiffer fibre, producing an increase in G_{12} modulus. This effect can also be seen by comparing the deterministic model and *S2-X* model fibre/matrix ratio of face reaction forces generated while resisting the shear strain. The *S2-X* model has a higher ratio indicating that fibre is contributing more in resisting the shear strain, compared with the deterministic model. In addition to face reaction forces, the same behaviour is seen with fibre/matrix strain energy ratio, as the ratio for the deterministic model is 0.48, whereas it increases to 0.55 for the *S2-X* model. Additionally, G_{13} experienced an increase of 2.5% with *S1-45* following the same reasoning as for G_{12}. It is found that the effective shape factors for G_{12} and G_{13} are specifically *S2* and *S1*, as each contributes in building the maximum distribution of fibre with 2 and 3-direction respectively, compared with the other shape uncertainties, *S3* and *S4* (refer to Fig. 3).

In terms of Poisson's ratio, maximum effects are a decrease of 5% for v_{23} and v_{32} by the *S3-45* combined uncertainties. For v_{32}, joint uncertainties increase the concentration of fibre phase in specific regions with respect to 2-direction (or 3- direction if considering v_{23} instead of v_{32}). The fibre material has a smaller Poisson's ratio and it is stiffer compared with matrix, resulting in a lower magnitude of transverse strain in the 2-direction compared with the centred fibre of the deterministic model.

After examining the full results (effect of individual geometrical uncertainties and all combinations), it is concluded that the geometric uncertainties that have the greatest effect on homogenised stiffness properties, compared with the deterministic model, are related to stacking uncertainty (*X* and *45*) rather than shape uncertainty factors (*S1, S2, S3* and *S4*).

4.1.2. Effect of material property uncertainty

The variation in fibre and matrix material stiffness has a direct effect on the overall RVE's elastic properties, as expected. In general, matrix material contributes most of the stiffness of the composite in all directions (except the 1-direction). Thus, it is not surprising that matrix uncertainty has a greater

influence on stiffness moduli, except for E_{11}, which is more dependent on the stiffer fibre. This can also be realised by examining the difference between E_{11} and E_{22} (or E_{33}) fibre/matrix stain energy ratio for any RVE, where it clearly shows that fibre has the higher strain energy in E_{11}, and the opposite in E_{22} (or E_{33}), see Fig. 7.

As for effects on Poisson's ratios, both material uncertainties show similar effect due to the fact that none purely dominate a direction as the fibre-volume ratio is approximately 50%. However, higher effects are seen in v_{21} and v_{31}. For v_{31}, increasing fibre stiffness reduces strains in 1-direction, resulting in decreased v_{31}. On the other hand, increasing matrix stiffness will reduce strains in 3-direction, leading to higher v_{31}. This same observation is also valid for v_{21}.

4.1.3. Sensitivity of material and geometrical uncertainties

Based on the 2^k sensitivity analysis summarised in Appendix 1(a-c), it can be seen that for E_{11} fibre uncertainty *F* has the most influence, as it is furthest from the theoretical normal distribution line. This is not surprising, as the results for individual uncertainties in Table 1 show that only fibre uncertainty *F* has a significant effect on E_{11}. Whereas E_{22} and E_{33} are sensitive to matrix *M* and stacking *45* uncertainties, since matrix phase is the main contributor to transverse Young's moduli, and *45* stacking geometrical uncertainty increases the role that the fibre plays in resisting the applied strain (as discussed above). It is important to note that the *S3-45* combination has the greatest increase on E_{22}, but it is insignificant as a combination because the major effect comes from *45* uncertainty rather than *S3* or both. This demonstrates the effectiveness of using factorial design method in analysing these factors and combinations.

On the other hand, for all three shear moduli, matrix uncertainty *M* has the greatest influence for the same reasons explained earlier in material uncertainties effect. Nevertheless, G_{23} is also sensitive to fibre uncertainty *F* to some extent. This can be explained by observing that the fibre/matrix elastic strain energy ratio for G_{23} is 0.66 (in the deterministic model), compared with only 0.48 for G_{12} (and G_{13}), making any change in fibre stiffness a more sensitive effect for G_{23}, see Fig. 8. However, although geometrical uncertainty, especially stacking *45*, has some influence on shear moduli (Table 2), this influence is much smaller compared with the sensitivity of the matrix stiffness.

As for the homogenised Poisson's ratios, in general, geometrical stacking uncertainty (*X* and *45*) dominated the effect on most ratios. Nevertheless, in v_{21} and v_{31} material property uncertainties are the most sensitive (see Appendix 1(g-l)). In both cases, an increase in fibre stiffness decreases the Poisson's ratio, whereas an increase in matrix stiffness has the opposite effect. This is because an increase in fibre stiffness reduces the magnitude of the transverse strain in the (transverse) 1-direction, whereas an increase in matrix stiffness reduces strain magnitude in the (normal) 2 and 3-directions.

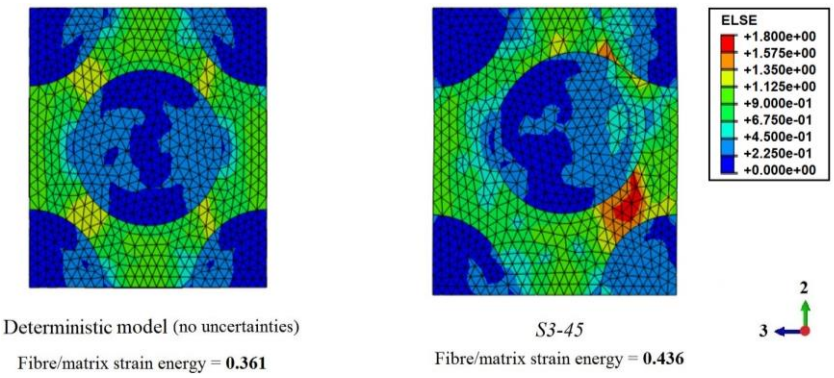

Fig. 6. The difference in fibre/matrix elastic strain energy (ELSE) ratio between the deterministic model and *S3-45* combined uncertainties for E_{22}.

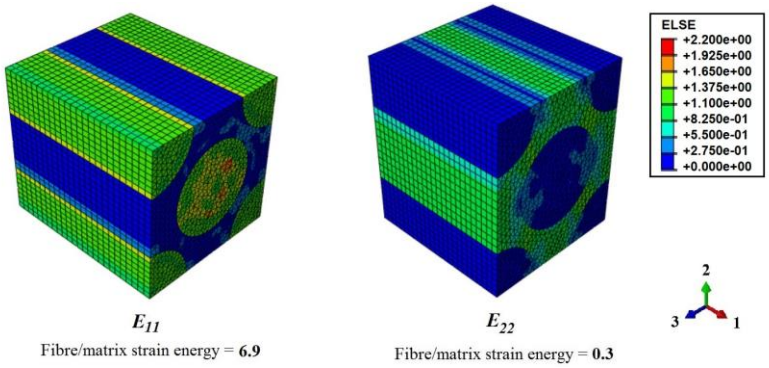

Fig. 7. The difference in fibre/matrix elastic strain energy (ELSE) ratio between E_{11} and E_{22} for the deterministic RVE.

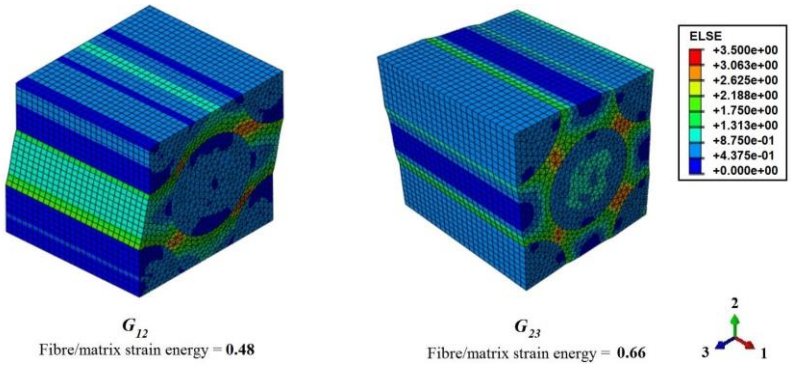

Fig. 8. The difference in fibre/matrix elastic strain energy (ELSE) ratio between G_{12} and G_{23} for the deterministic RVE.

4.2. Surrogate modelling

In order to improve the efficiency of the reliability analysis, it is necessary to minimise the use of FE RVE homogenisation analysis through the use computationally cheaper surrogate models. The latter are developed using polynomial regression fits to form the relationship between uncertainties and their effect on all elastic properties using data points obtained by the FE RVE homogenisation. For instance, the percentage of the effect on the elastic property against the increase of material stiffness property from 0% in the deterministic model to 2%, 4% and up to 5% (the upper bound) is a linear relationship, as shown in Fig. 9 (fibre response is similar to the presented matrix response). On the other hand, a second-order relationship for the effect of geometrical uncertainties *X* and *45* (see Fig. 10 for *45* uncertainty). This test reveals that the effects caused by these uncertainties are consistent and follow predictable patterns.

Further investigation of *F*, *M*, and *45* uncertainties identified that they have independent effects on the composites homogenised stiffness properties. Therefore, the total effect is the sum of individual effects from all uncertainties (see Eq. 1).

$$E_i = \bar{E}_i + \sum_{j=1}^{N} f_i(x_j) \qquad \text{Eq. 1}$$

Where E_i is one of the approximated elastic properties, $\bar{E}_i$ is the deterministic value, N the number of uncertain parameters (x_j) and $f_i(x_j)$ is a polynomial that links the value of uncertain parameter j with the change in elastic property i (relative to deterministic value).

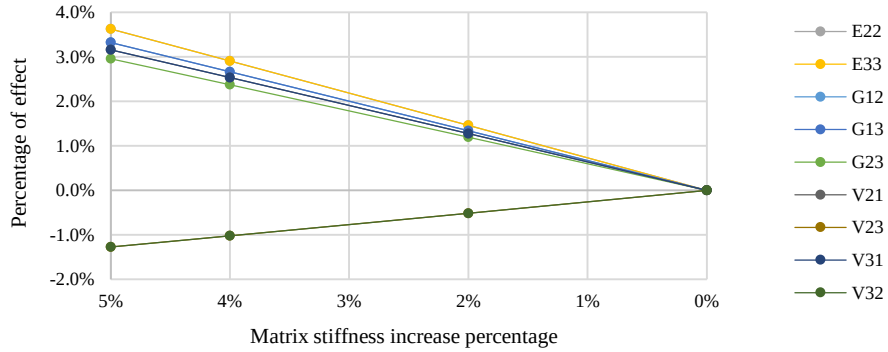

Fig. 9. Effect on elastic properties caused by increasing matrix stiffness (*M* uncertainty).

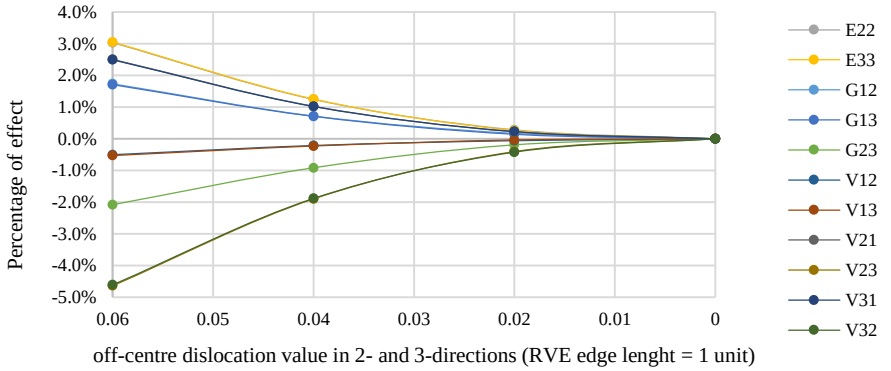

Fig. 10. Effect on elastic properties caused by shifting the fibre off-centre (*45* uncertainty).

To verify this, Table 3 shows excellent agreement between stiffness properties estimated by summing the effect of these three uncertainties plus the established deterministic model stiffness properties (see Fig. 13), against homogenised stiffness properties computed using FE analysis of an RVE that models the same uncertainties together. The same behaviour is observed if the effect of *X* and *Y* uncertainties are coupled. Aforementioned, *Y* uncertainty is shifting the central fibre in 2-direction instead of 3-direction (as in *X* uncertainty). For the reliability analysis, the *X* and *Y* uncertainties are transformed into a polar coordinate system (defined by r and θ). This enables establishing the effect caused by stacking uncertainty anywhere within a circular region around the centre of the RVE, instead of following deterministic paths of *X*, *Y*, or *45* uncertainties (see Fig. 11).

Table 3. Verification of uncertainties independent effect on the homogenised elastic properties.

		Accumulative homogenised property					**Homogenised property by FEA of an RVE modelled with: *F*, *M*, and *45***
Elastic property	**Unit**	**(1) RVE with *F* uncertainty**	**(2) RVE with *M* uncertainty**	**(3) RVE with *45* uncertainty**	**(4) Deterministic RVE***	**(1) + (2) + (3) – 2 × (4) Homogenised property**	
E_{11}	GPa	255.25	246.09	244.62	244.56	256.85	256.86
E_{22}		145.40	148.71	148.05	143.53	155.10	155.45
E_{33}		145.39	148.70	148.04	143.52	155.09	155.44
G_{12}	GPa	65.83	66.91	66.09	64.78	69.27	69.40
G_{13}		65.83	66.90	66.09	64.78	69.27	69.40
G_{23}		71.21	71.90	68.38	69.85	71.80	71.80
v_{12}	ratio	0.175	0.176	0.174	0.175	0.174	0.174
v_{13}		0.175	0.176	0.174	0.175	0.174	0.174
v_{21}		0.100	0.106	0.106	0.103	0.106	0.106
v_{23}		0.349	0.341	0.328	0.345	0.328	0.328
v_{31}		0.100	0.106	0.106	0.103	0.106	0.106
v_{32}		0.349	0.340	0.328	0.345	0.328	0.328

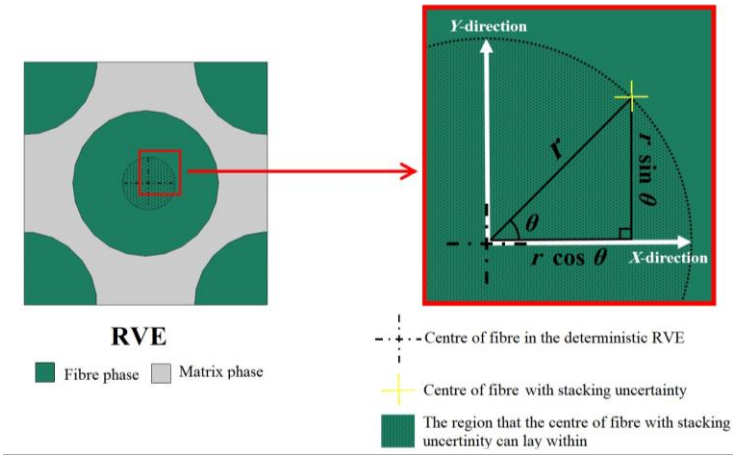

Fig. 11. Stacking uncertainty transformation from Cartesian to polar coordinate system.

To summarise, two types of surrogate models are used: polynomial-based surrogate models to obtain the dependant homogenised effective elastic properties at any independent uncertainty value, and accumulation of independent effects to build-up the overall effective elastic properties. Exploiting these behaviours the homogenised elastic properties for any random combination of uncertainties are immediately obtained without the need to generate and run computationally expensive numerical models. These surrogate models enable the use of MCS reliability analysis to quickly and accurately estimate probabilities of failure.

4.3. Uncertainties effect on reliability

Based on effects and sensitivity of the studied uncertainties and their combinations, it is concluded that material property uncertainties (*F* and *M*) and fibre stacking uncertainties (*X* and *45*) are the most influential. Whereas, the assumed shape uncertainties are not as significant. Therefore, in the reliability analysis study, shape variations are omitted by assuming that all fibres have circular cross-sections. The effect of the most influential uncertainties on the performance of composite structures is assessed by three criteria: buckling, vibration, and bending; because these properties form the overall stiffness behaviour of a composite [13]. MCS is used to compute probabilities of failure for the three performance criteria by assuming failure occurs once serviceability limits are reached, the assumed limits and formulation of the limit state function (LSF) for each criterion is detailed in Eqs. 2-4 [13, 32, 33]. The example selected to identify the probabilities of failure is a set of four specially orthotropic 0.5 mm thick laminas, symmetrically arranged about the laminate mid-surface (see Fig. 12), its serviceability limits are selected to reflect reasonable probabilities of failure. For this particular configuration, the required stiffness components are only D_{11}, D_{12}, D_{22} and D_{66}, hence, simplifying LSF calculations.

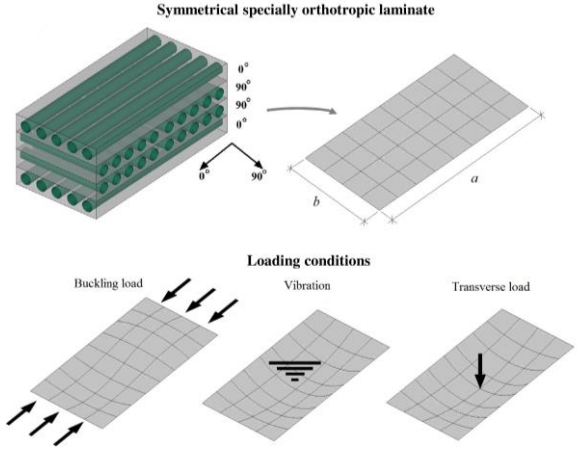

Fig. 12. Symmetrically specially orthotropic laminate subjected buckling, vibration, and bending loading conditions.

$$g_b(X) = N - N_{LS} = \pi^2 \left[D_{11} \left[\frac{m}{a}\right]^2 + 2(D_{12} + 2D_{66}) \left[\frac{n}{b}\right]^2 + D_{22} \left[\frac{n}{b}\right]^4 \left[\frac{a}{m}\right]^2 \right] - N_{LS} \quad \text{Eq. 2}$$

$$g_f(X) = \omega^2 - \omega^2{}_{LS} = \frac{\pi^4}{\rho} \left[D_{11} \left[\frac{m}{a}\right]^4 + 2(D_{12} + 2D_{66}) \left[\frac{m}{a}\right]^2 \left[\frac{n}{b}\right]^2 + D_{22} \left[\frac{n}{b}\right]^4 \right] - \omega^2{}_{LS} \quad \text{Eq. 3}$$

$$g_d(X) = w_{LS} - w = w_{LS} - \frac{16 p_0}{\pi^6} \left[\frac{\frac{1}{mn} sin\frac{m\pi x}{a} sin\frac{n\pi y}{b}}{D_{11}\left[\frac{m}{a}\right]^4 + 2(D_{12}+2D_{66})\left[\frac{m}{a}\right]^2\left[\frac{n}{b}\right]^2 + D_{22}\left[\frac{n}{b}\right]^4} \right] \quad \text{Eq. 4}$$

The above applies for a simply supported symmetrical specially orthotropic laminate, where:

N, N_{LS}: Buckling load and its limit state value per laminate width ($1450\ N/mm$) respectively, at which a bifurcation in deformation path occurs

$\omega^2, \omega^2{}_{LS}$: Laminate natural frequency squared and its limit state value ($12.8/sec^2$) respectively

w, w_{LS}: Deflection by the imposed uniform transverse load and the maximum limit state deflection value ($0.8\ mm$) at the centre of laminate plate (x=a/2, y=b/2) respectively

p_0: Imposed uniform load $= 1.0\ MPa$

m, n: Number of half wavelengths in 0° and 90°-direction respectively. For vibration and bending m=n=1. Whereas, m=2 and n=1 for buckling

a, b: Laminate length ($100\ mm$), and width ($50\ mm$) respectively

D_{ij}: Laminate stiffness components, calculated using random variables, X through surrogate models and *[ABD]* matrix stiffness calculations

ρ: Laminate density $= 2.508\ g/cm^3$

In the above equations, X are the random variables relating to micro-scale uncertainties that affect the effective stiffness properties of the laminate. MCS is used to generate samples of X, which are used to compute effective elastic properties using surrogate models (explained in section 4.2). These are then used with classical lamination theory to calculate the D_{ij} stiffness terms and evaluate the LSFs and the probability of failure: $P_f = P[g(X) \leq 0]$. The proposed implementation of the LSFs, surrogate models, and the use of MCS are illustrated by the flowchart in Fig. 13.

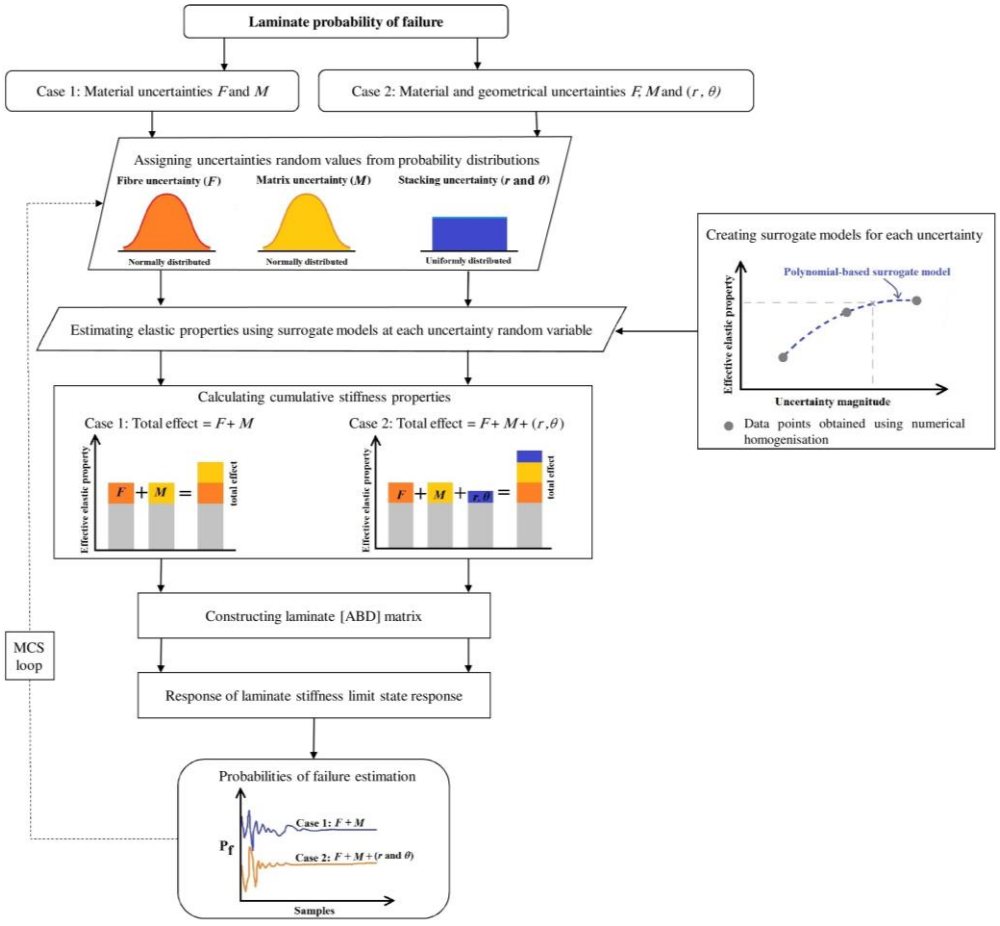

Fig. 13. Proposed framework flowchart for evaluating laminate probabilistic stiffness performance.

In the proposed reliability analysis (Fig. 13) two statistical distributions are assumed: a uniform distribution for fibre stacking is chosen based on observations from SEM images, and a normal distribution with 10% coefficient of variation is chosen for material property uncertainties. Results show that when geometric uncertainties are included, probabilities of failure are distinctively lower than when only material property uncertainties are considered (see Fig. 14). This is because modelling the geometric stacking uncertainty results in having stiffer homogenised properties (see Table 2), which increases the [*ABD*] matrix stiffness, leading to improved overall laminate stiffness response (i.e. lower deflection, higher critical buckling load, or higher fundamental natural frequency). On the other hand, the global sensitivity analysis indices show that material property uncertainties tend to be more sensitive to variation compared with stacking uncertainties (r and θ), (see Fig. 15). It is important to note that the sensitivity results obtained are mainly effected by the assumed range of statistical distribution. Altering distributions and coefficients of variation can effect global sensitivity analysis indices noticeably.

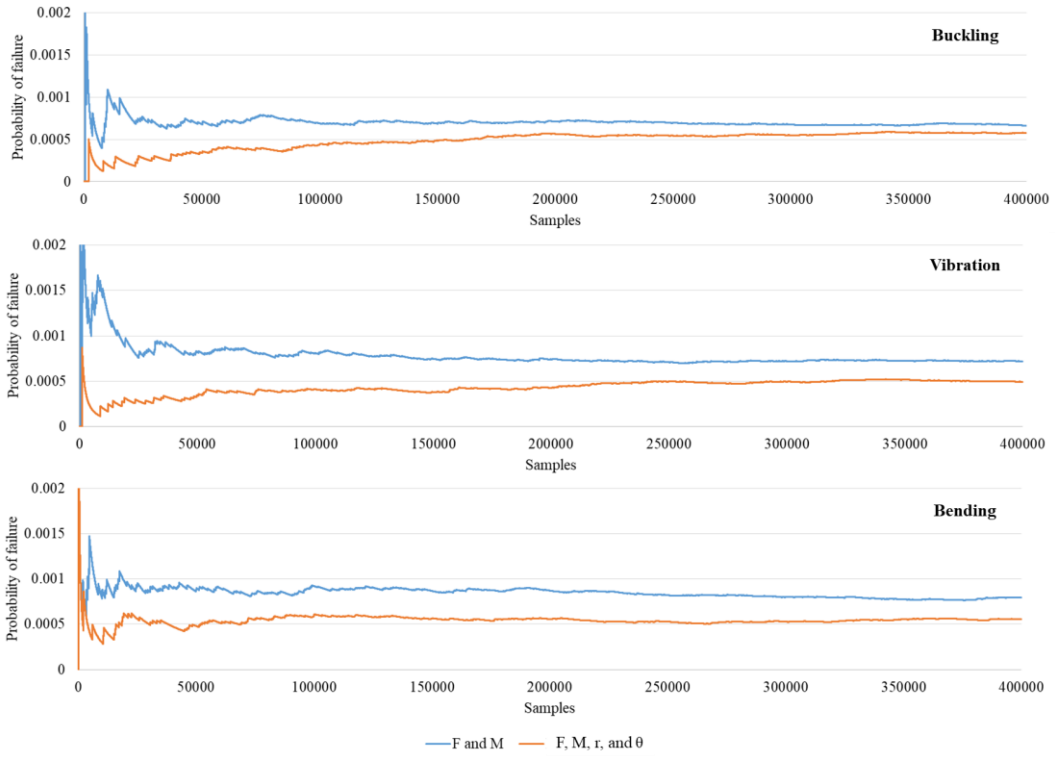

Fig. 14. Probabilities of failure for laminate modelled with: material property uncertainty (*F* and *M*), material and geometrical uncertainties (*F*, *M*, *r*, and θ).

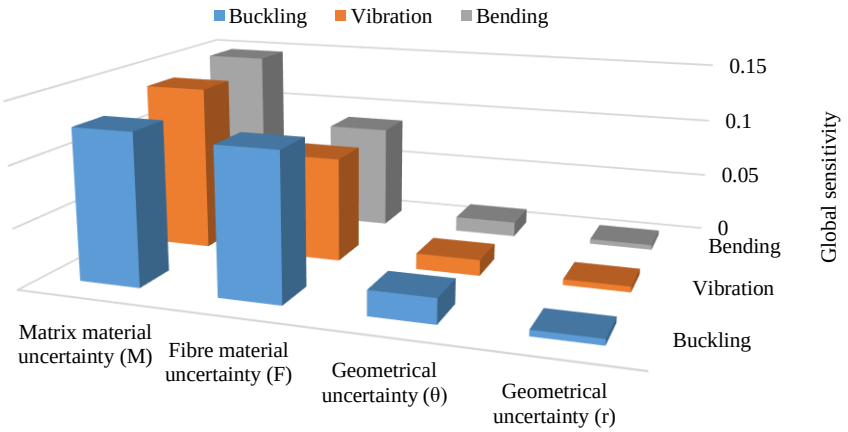

Fig. 15. Global sensitivity indices for *F*, *M*, *r*, and θ uncertainties.

5. Conclusions

This study examines the significance of material and geometrical uncertainties on fibre reinforced composite stiffness properties. The first objective is to find which uncertainties have a significant influence on effective elastic properties. Thus, effect magnitudes and sensitivities of identified uncertainties on effective elastic properties are estimated using a periodic RVE homogenisation method and a factorial design method; the main findings are:

- Young's modulus E_{11} is mainly affected by fibre material property uncertainty (*F*). Whereas, for transverse Young's moduli E_{22} and E_{33}, stacking uncertainties (*X* and *45*) show considerable effect and sensitivity that exceed fibre material property uncertainty, and close to matrix material property uncertainty;
- Shear moduli are mainly affected by matrix material stiffness uncertainty (*M*), followed by the fibre stacking uncertainty, then fibre stiffness uncertainty;
- Most Poisson's ratios are considerably affected by geometrical uncertainty, apart from two ratios that were affected more by constituent material properties;
- Shape uncertainties were significantly less influential, compared with other uncertainties.

The above uncertainty/property effect and sensitivity rankings are summarised in the matrix below:

		Material uncertainty		**Geometrical uncertainty**	
		Fibre stiffness (*F*)	**Matrix stiffness (*M*)**	**Fibre stacking (*X* and *45*)**	**Fibre shape (S_1, S_2, S_3,S_4)**
Young's moduli	E_{11}	High	Very low	No effect	No effect
	E_{22}, E_{33}	Moderate	High	High	Very low
Shear moduli		Low	High	Moderate	Very low
Poisson's ratios		Moderate	Moderate	High	Very low

Based on first phase findings, the reliability analysis study considered stacking uncertainty (combination of *X* and *Y*) along with both fibre and matrix uncertainties (*F* and *M*) to evaluate their effect on the reliability of a symmetric laminate for buckling, vibration and bending criteria. It was also found that that the above uncertainties have completely independent effects on the elastic properties of composites. This behaviour was employed to develop efficient polynomial-based surrogate models that estimate the effect of any combination of uncertain values, without the need to generate and run expensive numerical models. Results from the reliability analysis show that:

- The probability of failure decreases when the laminate is analysed with stacking geometrical uncertainty, because of increased homogenised stiffness properties;
- The probability of failure is less sensitive to the uniform geometrical uncertainty variation compared with the normally distributed constituent material property uncertainties.

To conclude, this study confirms that not only material property uncertainties have a significant effect on the homogenised elastic properties of fibre reinforced composites, but fibre stacking geometrical uncertainty is also influential. Therefore, it is necessary to account for and propagate the effect of stacking geometrical uncertainty when estimating the effective elastic properties and generalising it to higher scales. This can be done efficiently by exploiting the independence of the effect of material and geometrical uncertainties to develop polynomial-based surrogate models.

Acknowledgements

This work was supported by the University of Aberdeen Elphinstone scholarship scheme.

References

[1] Komeili M, Milani AS (2012) The effect of meso-level uncertainties on the mechanical response of woven fabric composites under axial loading. Comput Struct 90–91:163-171. http://dx.doi.org/10.1016/j.compstruc.2011.09.001

[2] Zhu T (1993) A reliability-based safety factor for aircraft composite structures. Computers & Structures 48(4):745-748. https://doi.org/10.1016/0045-7949(93)90269-J

[3] British Standards Institution (1987) BS 4994:1987 Specification for design and construction of vessels and tanks in reinforced plastics

[4] Hill R (1963) Elastic properties of reinforced solids: Some theoretical principles. Journal of the Mechanics and Physics of Solids 11(5):357-372. http://dx.doi.org/10.1016/0022-5096(63)90036-X

[5] Zhou X, Gosling PD, Ullah Z et al (2017) Stochastic multi-scale finite element based reliability analysis for laminated composite structures. Appl Math Model 45:457-473. http://doi.org/10.1016/j.apm.2016.12.005

[6] Brockenbrough JR, Suresh S, Wienecke HA (1991) Deformation of metal-matrix composites with continuous fibers: geometrical effects of fiber distribution and shape. Acta Metallurgica et Materialia 39(5):735-752. https://doi.org/10.1016/0956-7151(91)90274-5

[7] Nikopour H (2013) A virtual frame work for predication of effect of voids on transverse elasticity of a unidirectionally reinforced composite. Computational Materials Science 79:25-30. http://dx.doi.org/10.1016/j.commatsci.2013.05.049

[8] Huang Y, Jin KK, Ha SK (2008) Effects of fiber arrangement on mechanical behavior of unidirectional composites. J Composite Mater 42(18):1851-1871. 10.1177/0021998308093910

[9] Wang C, Zhong Y, Bernad Adaikalaraj PF et al (2016) Strength prediction for bi-axial braided composites by a multi-scale modelling approach. J Mater Sci 51(12):6002-6018. 10.1007/s10853-016-9901-z

[10] Xia Z, Zhang Y, Ellyin F (2003) A unified periodical boundary conditions for representative volume elements of composites and applications. International Journal of Solids and Structures 40(8):1907-1921. https://doi.org/10.1016/S0020-7683(03)00024-6

[11] Montgomery D,C. (2008) Design and Analysis of Experiments, 7 edn. John Wiley & Sons

[12] Callister WD, Rethwisch DG (2014) Materials Science and Engineering: An Introduction, 9th edition edn. Wiley, Hoboken, NJ

[13] Jones RM (1999) Mechanics of composite materials. Brunner-Routledge, New York ; London

[14] Sriramula S, Chryssanthopoulos MK (2009) Quantification of uncertainty modelling in stochastic analysis of FRP composites. Composites Part A: Applied Science and Manufacturing 40(11):1673-1684. https://doi.org/10.1016/j.compositesa.2009.08.020

[15] Bogdanor MJ, Oskay C, Clay SB (2015) Multiscale modeling of failure in composites under model parameter uncertainty. Comput Mech 56(3):389-404. 10.1007/s00466-015-1177-7

[16] Sobol′ IM (2001) Global sensitivity indices for nonlinear mathematical models and their Monte Carlo estimates. Mathematics and Computers in Simulation 55(1):271-280. https://doi.org/10.1016/S0378-4754(00)00270-6

[17] Cannavó F (2012) Sensitivity analysis for volcanic source modeling quality assessment and model selection. Computers & Geosciences 44(Supplement C):52-59. https://doi.org/10.1016/j.cageo.2012.03.008

[18] Ji X, Wang C, Francis BAP et al (2015) Mechanical and Interfacial Properties Characterisation of Single Carbon Fibres for Composite Applications. Exp Mech 55(6):1057-1065. 10.1007/s11340-015-0007-3

[19] González C, LLorca J (2007) Mechanical behavior of unidirectional fiber-reinforced polymers under transverse compression: Microscopic mechanisms and modeling. Composites Sci Technol 67(13):2795-2806. http://dx.doi.org/10.1016/j.compscitech.2007.02.001

[20] Nikopour H, Selvadurai APS (2014) Concentrated loading of a fibre-reinforced composite plate: Experimental and computational modeling of boundary fixity. Composites Part B: Engineering 60:297-305. http://dx.doi.org/10.1016/j.compositesb.2013.12.034

[21] Qiu S, Fuentes CA, Zhang D et al (2016) Wettability of a single carbon fiber. Langmuir 32(38):9697-9705. 10.1021/acs.langmuir.6b02072

[22] Ferreira RTL, Rodrigues HC, Guedes JM et al (2014) Hierarchical optimization of laminated fiber reinforced composites. Composite Structures 107:246-259. https://doi.org/10.1016/j.compstruct.2013.07.051

[23] Young W,Kwon, David H,Allen, Ramesh T (2010) Multiscale Modeling and Simulation of Composite Materials and Structures. Springer, Boston, MA, New York

[24] Cheng G-, Cai Y-, Xu L (2013) Novel implementation of homogenization method to predict effective properties of periodic materials. Acta Mechanica Sinica/Lixue Xuebao 29(4):550-556. 10.1007/s10409-013-0043-0

[25] Zhou X, Gosling PD, Ullah Z et al (2016) Exploiting the benefits of multi-scale analysis in reliability analysis for composite structures. Composite Structures 155:197-212. http://dx.doi.org/10.1016/j.compstruct.2016.08.015

[26] Geers MGD, Kouznetsova VG, Brekelmans WAM (2010) Multi-scale computational homogenization: Trends and challenges. J Comput Appl Math 234(7):2175-2182. http://dx.doi.org/10.1016/j.cam.2009.08.077

[27] Naik RA, Crews JH (1993) Micromechanical Analysis of Fiber-Matrix Interface Stresses Under Thermomechanical Loadings. Composite Materials: Testing and Design 11. 10.1520/stp12629s

[28] Sun CT, Vaidya RS (1996) Prediction of composite properties from a representative volume element. Composites Science and Technology 56(2):171-179. https://doi.org/10.1016/0266-3538(95)00141-7

[29] Bonora N, Ruggiero A (2006) Micromechanical modeling of composites with mechanical interface – Part II: Damage mechanics assessment. Composites Science and Technology 66(2):323-332. https://doi.org/10.1016/j.compscitech.2005.04.043

[30] Omairey SL, Dunning PD, Sriramula S (2018) Development of an ABAQUS plugin tool for periodic RVE homogenisation. Engineering with Computers. https://doi.org/10.1007/s00366-018-0616-4

[31] Sadd MH (2014) Chapter 6 - Strain Energy and Related Principles. In: Sadd MH (ed) Elasticity (Third Edition). Academic Press, Boston, pp 119-139

[32] Reddy J,N. (2004) Mechanics of laminated composite plates and shells: theory and analysis. Ringgold Inc, Portland, United States, Portland

[33] Buragohain M,K. (2017) Composite Structures: Design, Mechanics, Analysis, Manufacturing, and Testing, 1 edn. CRC Press, Boca Raton

Appendix 1: Normal probability plots of the 2^k factorial design for all uncertainties and combinations.

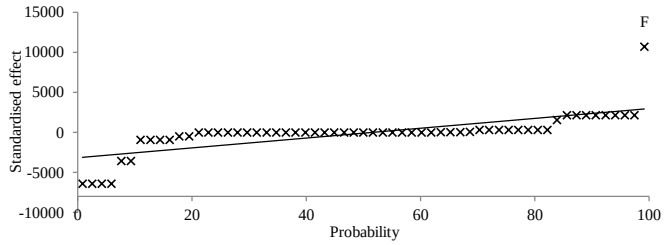

(a) E_{11} normal distribution probability- standardised effect plot.

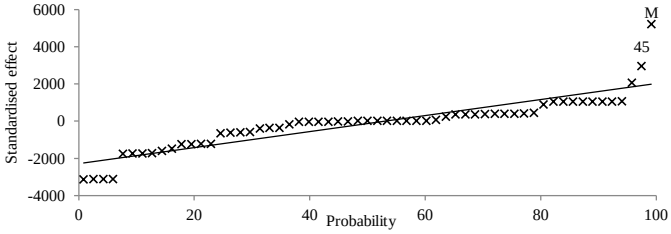

(b) E_{22} normal distribution probability- standardised effect plot.

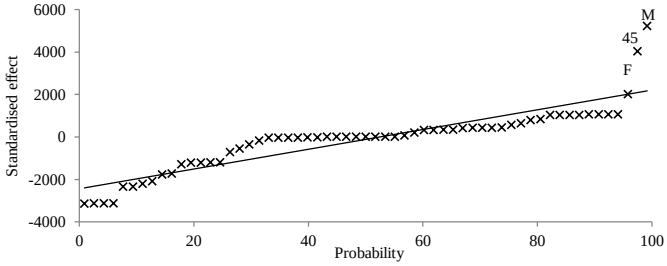

(c) E_{33} normal distribution probability- standardised effect plot

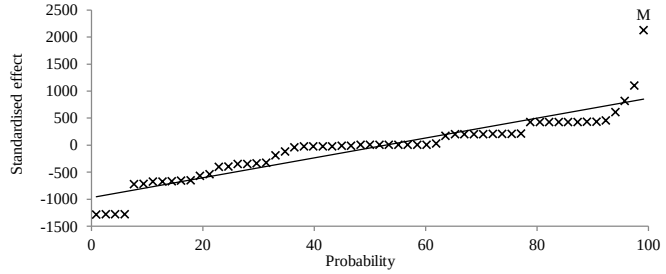

(d) G_{12} normal distribution probability- standardised effect plot.

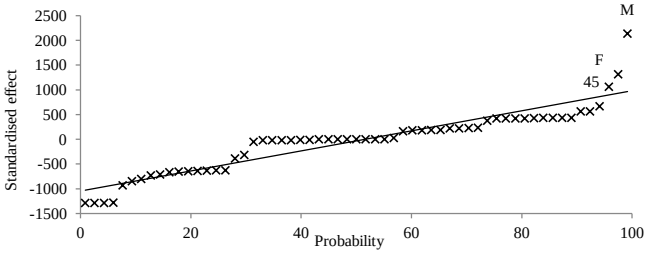

(e) G_{13} normal distribution probability- standardised effect plot.

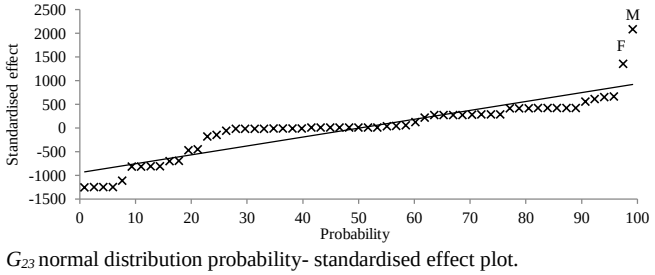

(f) G_{23} normal distribution probability- standardised effect plot.

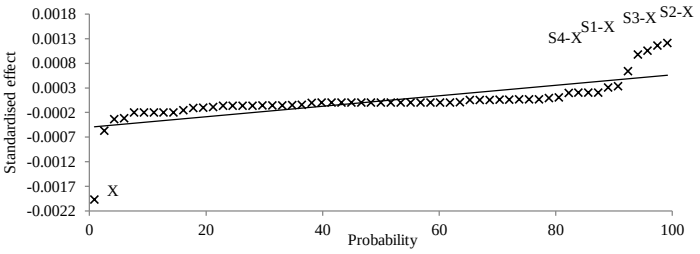

(g) v_{12} normal distribution probability- standardised effect plot.

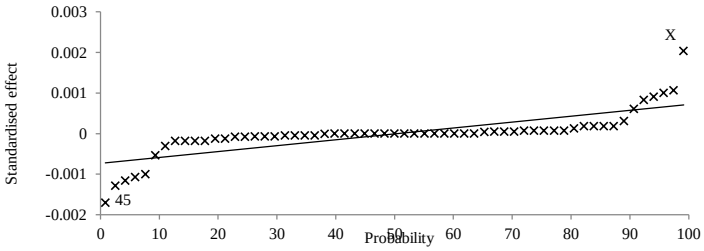

(h) v_{13} normal distribution probability- standardised effect plot.

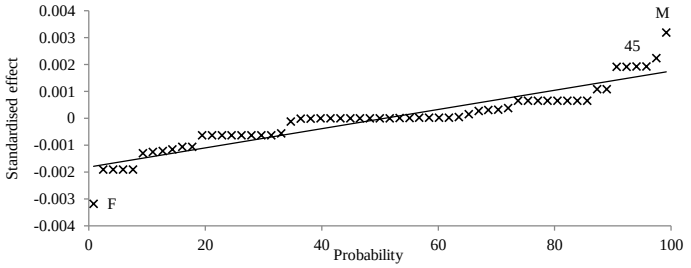

(i) v_{21} normal distribution probability- standardised effect plot.

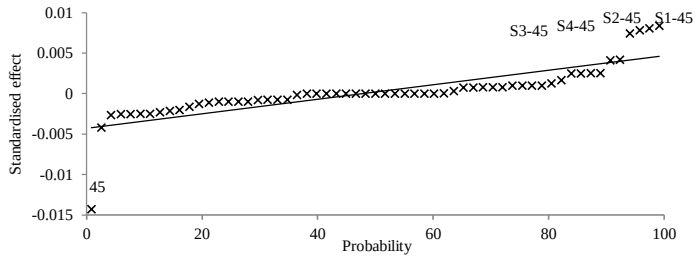

(j) v_{23} normal distribution probability- standardised effect plot.

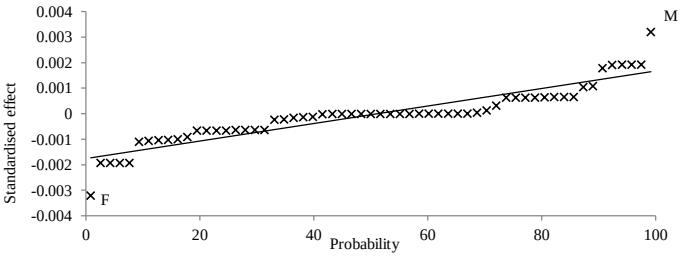

(k) v_{31} normal distribution probability- standardised effect plot.

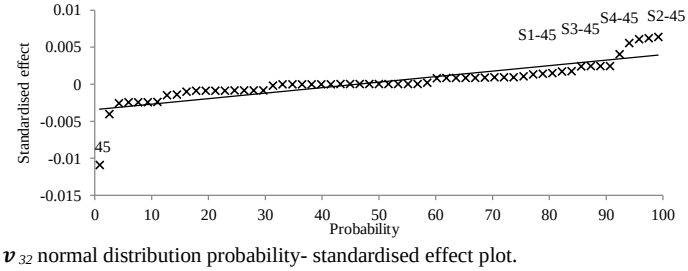

(l) v_{32} normal distribution probability- standardised effect plot.